Theor Chem Acc (2000) 104:40–49
DOI 10.1007/s002149900092

Theoretical
Chemistry Accounts

Regular article

Non adiabatic vibrational resonances in molecules containing low barrier moieties: a classical dynamics study

Sergio Abbate, Enrico Montagnoli, Giovanna Longhi

Dipartimento di Scienze Biomediche e Biotecnologie, Università di Brescia, via Valsabbina 19, I-25123 Brescia, Italy
and INFM, UDR Brescia, Italy

Received: 28 April 1999 / Accepted: 21 September 1999 / Published online: 15 December 1999
© Springer-Verlag 2000

Abstract. We discuss the classical dynamics of a CH-stretching and an OH-stretching vibration coupled to a hindered rotation around a CC (OC) bond of a CH_3 group or an OH group. Our model is based on a two-dimensional system, in which zero angular momentum is assumed. The model is further simplified by considering only kinetic coupling between the CH (OH) stretching and the hindered rotation. Through numerical calculations, a new set of states is found, which originates from $n:1$ resonances between the internal rotation frequency and the stretching frequency, n being associated to the order of symmetry ($n = 3$ and 6 for the cases investigated). We also present a perturbative approach based on the Lie series method, which provides insight into these nonadiabatic states.

Key words: Local modes – Poincaré surfaces of section – Power spectrum – Nonadiabatic effects – Lie series

1 Introduction

The vibrational spectroscopy of molecules containing methyl groups has attracted the interest of many authors, since the large amplitude torsional modes around the CC bond provide a dense manifold of states that has a great influence on other vibrational states and/or on the dynamics of the molecules. In particular we refer here to the work of Cavagnat and coworkers [1–3], who have discussed the signatures of torsional and rotational CH_3 (and CHD_2 and, recently, CH_2D) states in the CH-stretching region of molecules such as toluene and nitromethane (either fundamental or overtones). Many other authors have contributed to these studies, both experimentally and theoretically [4], with the aim of understanding the importance of ''dark states'' in methyl-containing molecules. It is also worthwhile mentioning the works of Moss and coworkers [5], who have discussed the role of internal rotation in the acceleration of dynamical and/or internal vibrational relaxation (IVR) processes. With the same motivations, high-resolution and high-overtones spectroscopy of methanol has recently been carried out [6, 7].

The quantum mechanical model that Cavagnat and Lascombe [1] devised for the interpretation of the CH-stretching fundamental region and successively applied to the overtone region [2] is based on the adiabatic separation of the stretching mode from the hindered rotation. It has been fruitfully used to interpret vibrational spectra up to the fifth stretching overtone ($\Delta v = 6$), with some significant but nonessential perturbations coming from Fermi resonance interactions between CH stretching and HCC bending. Recent works on methanol follow essentially the same lines [6, 7], even though some nonadiabatic effects have been explicitely pointed out by Rizzo and coworkers [7] (i.e. the dependence of CH-stretching frequencies on kinetic energy terms associated with hindered rotation). The existence of more dramatic nonadiabatic effects can be expected on the basis of general considerations. Following, for example, Dittrich and Reuter [8], one can accept that a rotating frame of reference (such as a rotating methyl group) may perturb higher energy vibrations contributing a geometric (Berry) phase.

In the model we discuss here, we follow the common assumption of zero angular momentum, as has been done in this same context by Cavagnat and coworkers [1–3] and by Shranz and Collins [9] for hydrogen peroxide type molecules. This has been done, even though torsion–rotation coupling terms have been demonstrated to be quite important [4, 10]. The model we treated is a two degrees of freedom model system composed of a Morse-type CH-stretching oscillator and a torsional/rotational oscillator, coupled exclusively through a kinetic energy term. In other words we ignore the dependence of the torsional hindering potential on the stretching action or, correspondingly, of the stretching fundamental and overtone frequencies on the torsional angle. Such dependences have been documented in the literature [1, 11]. We have examined this system by classical mechanics through numerical solutions of

Correspondence to: S. Abbate

Hamilton equations, taking advantage especially of graphic procedures such as Poincaré surfaces of section (PSS) [12], plots of the trajectories in the configuration space (Lissajous-type maps), plots of the time evolutions of the two oscillators' energies versus time, and finally of power spectra of the electric dipole moment [13]. Finally, we carried out a classical perturbation analysis [14] of the system, by which we rationalize semi-quantitatively the results that were obtained numerically.

2 Discussion of the model: numerical results and perturbative approach

We have introduced the Hamiltonian function

$$H = (p^2/2m) + hcD\{1 - \exp[-a(l - l_0)]\}^2 + p_\varphi^2/2\mathscr{I} + hc(V/2)(1 - \cos n\varphi) \ , \quad (1)$$

where l is the CH (OH) bond length coordinate (l_0 being the equilibrium length), p is its conjugate momentum, φ is the hindered rotation coordinate, and p_φ is the corresponding conjugate momentum. The product hc of the Planck constant times the speed of light allows the parameters D and V to be expressed in wavenumber units. The dissociation constant, D, and the characteristic parameter, a, of the Morse potential are related to the mechanical frequency, ω, and the anharmonicity constant, χ, by the relations

$$D = \omega^2/4\chi \text{ and } a = \sqrt{8\pi^2 mc\chi/h} \ , \quad (2)$$

where m is the mass of the hydrogen atom. V is the height of the barrier to rotation of the methyl group.

The integer n is typical of the symmetry of the interaction of the methyl group with the rest of the molecule: $n = 6$ describes the behavior of a methyl group in the presence of a planar group, such as a phenyl or a nitro group, as discussed by Cavagnat and Lascombe [1], and $n = 3$ is typical of methanol [6, 7]. In Eq. (1) $\mathscr{I}$ is the moment of inertia for the torsion. When studying the torsion of one group with respect to another, one should take for $\mathscr{I}$ the reduced moment of inertia of the two groups, if one disregards all other vibrational degrees of freedom and the overall rotation. In the case of nitromethane and toluene (hereafter called system 1), for motion about the NC bond or the CC bond, $\mathscr{I}$ is the reduced moment of inertia of the methyl group and of the nitro and benzyl groups, respectively; however, since the latter groups have high moments of inertia, $\mathscr{I}$ is approximated by the moment of inertia of the methyl group, i.e.

$$\mathscr{I} = ml^2 \sin^2\theta + ml_0^2 \sin^2\theta + ml_0^2 \sin^2\theta \ , \quad (3)$$

where θ is the NCH angle for nitromethane and the CCH angle for toluene. We notice that just one CH bond of the methyl group is allowed to vary during torsion. In the case of methanol (called system 2 hereafter) we have used the reduced moment of inertia of the OH bond and the CH_3 group, namely

$$\mathscr{I} = \mathscr{I}_{OH}\mathscr{I}_{CH_3}/(\mathscr{I}_{OH} + \mathscr{I}_{CH_3}) \ , \quad (4)$$

where $\mathscr{I}_{CH_3}$ is the same as in Eq. (3) and $\mathscr{I}_{OH} = ml_{OH^2} \sin^2\alpha$, where α is the valence angle HOC. When we studied the influence of the CH_3 hindered rotation on CH stretchings, we allowed l to vary in Eq. (3) and kept l_{OH} fixed in Eq. (4). When we studied the influence of the CH_3 hindered rotation on the OH stretching, we kept $l = l_0$ in Eq. (3) and allowed l_{OH} to vary in Eq. (4). The kinetic energy term $(p_\varphi^2/2\mathscr{I})$ is the approximation of the expression of the kinetic energy by the usual G-matrix formalism [15] under the hypothesis that $m_H \ll m_C$ or m_O.

In what follows we used the values $\theta = 109.47°$ and $\alpha = 105°, m = 1$ amu, $l_0 = 1$ Å, and $l_{OH} = 1$ Å. Of course, a different choice of the masses allows CHD_2 or CH_2D to be treated as well. To deal with toluene and nitromethane, we used $\omega = 3000\,cm^{-1}$ and $\chi = 60\,cm^{-1}$. All these values are in the range of the true experimental values, even though they are not exact; however, they account for the quality of the phenomena observed. Moreover we do not rule out the existence of coupling terms in the potential energy, rather we want to emphasize the importance of some nonadiabatic effect due to velocity terms, in a way that was not explicitly considered by Cavagnat and coworkers [1–3] in CHD_2 (we will see later that their assumption is correct for CHD_2 but not for CH_3). We have tried three values for the barrier height, V, namely $V = 5\,cm^{-1}$ (close to that of nitromethane and toluene) [1], $V = 50\,cm^{-1}$ (close to that of 2,6-difluorotoluene) [16], and $V = 200\,cm^{-1}$ (the closest instance that we may cite is that of α-picoline reported by Cavagnat and Lautie [17]). For methanol, instead, we studied both the OH-stretching region and the CH-stretching region. In the former case we used $\omega_0 = 3811.2\,cm^{-1}$ and $\chi = 86.2\,cm^{-1}$ [18]; in the latter case we used $\omega_0 = 3000\,cm^{-1}$ and $\chi = 60\,cm^{-1}$. In both cases $V = 363\,cm^{-1}$ was assumed from the papers of Rizzo and coworkers [7].

2.1 Numerical calculations

In order to study the transition $0 \to v$, for the CH stretching in both system 1 and in system 2, we studied all the PSS obtained by numerical integration of the classical equations of motion based on the fourth-order Runge–Kutta algorithm. The following values of the total energy, E, were considered: 2940, 4365, 5760, 7125, 8460, 9765, 11040, 12285, and $13500\,cm^{-1}$. Instead, in order to describe the OH-stretching region for methanol (in system 2), we used the following values of E: 3725, 5523.3, 7277.60, 8989.25, 10657.80, 12283.25, 13865.60, 15404.85, and $16901.00\,cm^{-1}$. Such values are obtained by substituting $v^* = (v/2)$, from $v = 1$ to $v = 9$, into the relation $E_v = \omega(v^* + 1/2) - \chi(v^* + 1/2)^2$ as prescribed by the correspondence principle [19]: this principle states that the classical trajectory labeled by the average action value $v/2$ corresponds to the quantum transition $0 \to v$.

We report in Fig. 1 the results for the PSS for system 1 at $v = 7 (E = 11040\,cm^{-1})$ for $V = 200$ and $V = 50\,cm^{-1}$ for the two phase-space hyperplanes (φ, p_φ) and (l, p). The PSS in the (φ, p_φ) plane is obtained with condition $l = l_0, p > 0$; the second one, in the (l, p)

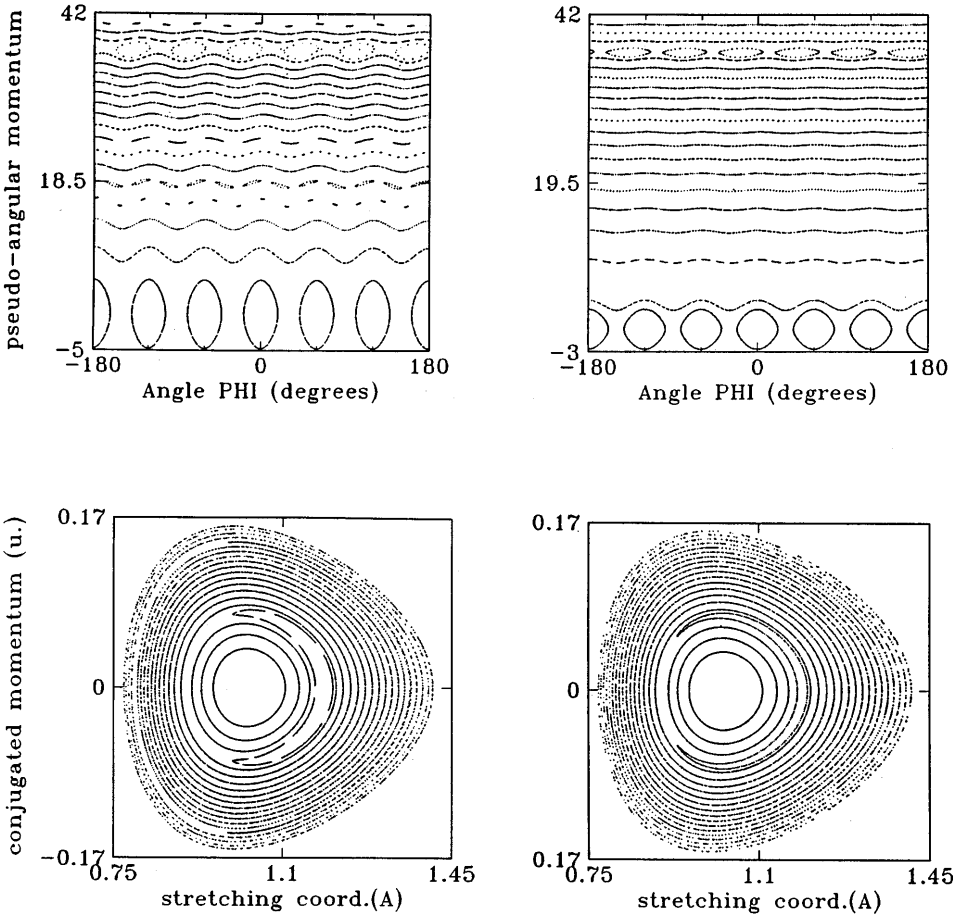

Fig. 1. Poincaré surfaces of section (*PSS*) obtained for the value $E = 11040\,\mathrm{cm}^{-1}$ of the total energy, corresponding to the transition $\Delta v = 7$ for the CH stretching of system 1. The PSS are given in the (φ, p_φ) plane (*top*) and the (l, p) plane (*bottom*). The results for the barrier highet $V = 200\,\mathrm{cm}^{-1}$ are given on the *left* and the results for $V = 50\,\mathrm{cm}^{-1}$ are given on the *right*. In each plot the 22 PSS curves differ for constant values in the initial energy difference $E_l - E_\varphi$ (see text). The pseudoangular momentum is in dimensionless units, the momentum conjugated to the stretching is in units of u. = amu Å(fs)$^{-1}$

plane, with the condition $\varphi = 0$ and $p_\varphi > 0$. The total integration time is of the order of 15,000 fs for each PSS curve. The different curves correspond to different initial values of the stretching and pseudorotational energies, E_l and E_φ, respectively defined as $E_l = (1/hc)(p^2/2m) + D\{1 - \exp[-a(l - l_0)]\}^2$ and $E_\varphi = (1/hc)p_\varphi^2/2\mathscr{I} + (V/2)(1 - \cos 6\varphi)$ equally spaced in $(E_l - E_\varphi)$. From the top PSS one may notice three types of curves, namely closed curves close to $p_\varphi = 0$, corresponding to librational or torsional oscillation of the methyl group, open curves, corresponding to rotational states of the methyl group, and, finally, sextuples of closed curves embedded in the methyl group rotational states. As it will be clear from the next paragraph, these curves correspond to 6:1 resonances. Other closed curves in the rotational ensemble can be found, but are hard to see on the scale of Fig. 1. Correspondingly, in the (l, p_l) plane there is no qualitative distinction between librational and rotational states; the former are the outer PSS curves, the latter the inner ones (bottom PSSs in Fig. 1). Instead, the third type of PSS curve is markedly different and corresponds to the evident banana-shaped curves. Such a qualitative aspect of the PSS figures is also found for $v = 6 (E = 9765\,\mathrm{cm}^{-1})$. The same qualitative aspect of the PSS is also found in methanol: we present in Fig. 2 the PSS relative to the (φ, p_φ) plane for the OH stretching (top) at $v = 9 (E = 16500\,\mathrm{cm}^{-1})$ and for the CH stretching at $v = 7 (E = 11040\,\mathrm{cm}^{-1})$. In these cases the most prominent resonances are 3:1, but 6:1, 9:1, and 9:2 resonances are also observed.

Certainly the most intriguing types of motion are the resonant ones: it turns out that they are still rotational states of the methyl (or OH) group with some peculiarities that are not present in the other rotational states. Considering system 1, we see that these new states appear in Fig. 1 for the initial condition $E_l = 2520\,\mathrm{cm}^{-1}$ and $E_\varphi = 8520\,\mathrm{cm}^{-1}$. Correspondingly, if one assumes that the energy E_φ is just that of a free rotator, namely $E_\varphi = (4\pi^2 c/h)(1/2)\mathscr{I}_0\omega_\mathrm{R}^2$, ($\mathscr{I}_0$ is the moment of inertia at the stretching equilibrium, namely $\mathscr{I}_0 = 3ml_0^2\sin^2\theta$) and if one calculates the stretching frequency from $\omega_\mathrm{S}(E_l) = [\omega_0^2 - 4\chi E_l]^{(1/2)}$, which is valid for the Morse potential, one finds that $\omega_\mathrm{R} = 463.6\,\mathrm{cm}^{-1}$ and $\omega_\mathrm{S} = 2862\,\mathrm{cm}^{-1}$. This demonstrates that they are close to 6:1 resonant states. Such resonances originate from a matching of the stretching frequency, ω_S, which is a decreasing function of the energy, with 6 times the rotation frequency, ω_R, which is an increasing function of the energy. The lowest energy at which these resonant modes are observed is that corresponding to the transition $\Delta v = 6$. Indeed in the approximation of separate degrees of freedom (so that the two expressions of E_l and E_φ just given are valid) the 6:1 resonance first appears when the total energy is concentrated on the pseudorotational degree of freedom, φ, and it is enough to give a frequency $\omega_\mathrm{R} \approx 500\,\mathrm{cm}^{-1}$, so that

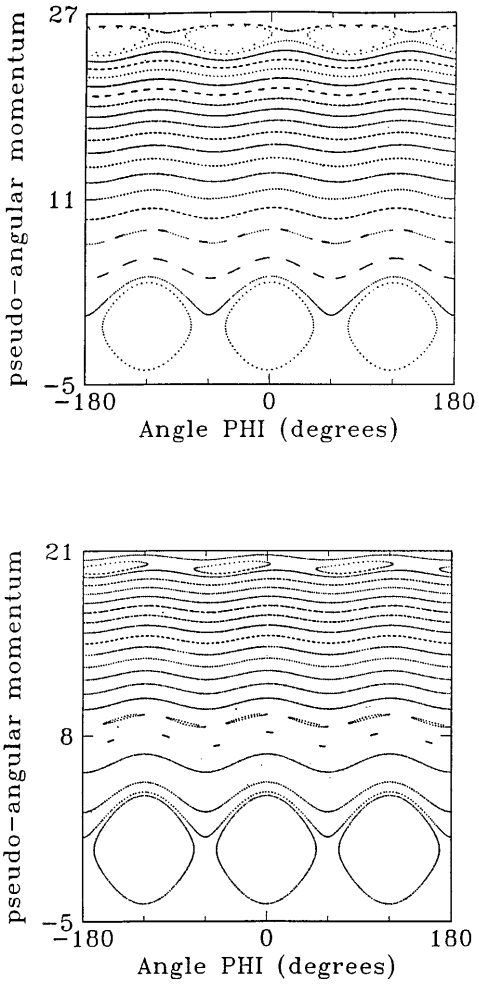

Fig. 2. PSS for system 2 obtained for the value $E = 16500\,\mathrm{cm}^{-1}$ of the total energy, corresponding to the transition $\Delta v = 9$ for the OH stretching (*top*) and for the value $E = 11040\,\mathrm{cm}^{-1}$, corresponding to the transition $\Delta v = 7$ for the CH stretching (*bottom*). The barrier height to rotation is $V = 363\,\mathrm{cm}^{-1}$. In each plot the 21 PSS curves differ for constant values in the initial energy difference $E_l - E_\varphi$ (see text). The pseudoangular momentum is in dimensionless units

$\omega_R = (1/6)\omega_0$. This happens when the total energy is $9884\,\mathrm{cm}^{-1}$. Integrating the exact Hamiltonian, we find the resonance at a slightly lower energy. At this point it is worthwhile pointing out that due to the dependence of ω_R on $\mathscr{I}_0$, ω_R decreases with increasing $\mathscr{I}_0$ at fixed energy: this is the reason why for CHD_2 and CH_2D such resonances are not found for the values of v investigated for system 1.

In the above considerations no use has been made of the parameter V. The existence of the resonant modes and the position of the stable and unstable fixed points corresponding to the simply periodic trajectories of the exact resonant condition are independent of V. We verified numerically that the resonances are still present also for $V = 5\ \mathrm{cm}^{-1}$, even though they are hard to notice on the scale of Fig. 1. V determines just the width of the resonance region in phase space. Corresponding to the 6:1 resonance, the stable fixed points are found precisely at $(\varphi = -18.3^\circ + k \cdot 60^\circ,\ k = 0, \pm 1, \pm 2, 3;\ p_\varphi = 36.92)$ and at $(l = 1.2\ \text{Å}, p = 0)$ and the unstable ones are found at $(\varphi = 11.7^\circ + k \cdot 60^\circ, k = 0, \pm 1, \pm 2, 3;\ p_\varphi = 36.92)$ and at $(l = 0.9\ \text{Å}, p = 0)$ (notice that the values of p_φ are in dimensionless units, that is to say in units of $\hbar$, for better comparison with the perturbative theory described later). Above the threshold value of $v(v = 6)$ where the resonances are found, the values of the fixed points are independent of the overtone order, v, and this further confirms the above interpretation. Analogous results are found for methanol (Fig. 2): the 3:1 resonances start from $v = 9$ for the OH stretching and $v = 7$ for the CH stretching. The stable and unstable fixed points are found at $(\varphi = -40.0^\circ + k \cdot 120^\circ, k = 0, \pm 1; p_\varphi = 25.02)$ and $(\varphi = +20.0^\circ + k \cdot 120^\circ, k = 0, \pm 1; p_\varphi = 25.02)$, respectively, for the OH stretching and at $(\varphi = -40.0^\circ + k \cdot 120^\circ, k = 0,\ \pm 1; p_\varphi = 19.83)$ and at $(\varphi = +20.0^\circ + k \cdot 120^\circ, k = 0,\ \pm 1; p_\varphi = 19.83)$, respectively, for the CH stretching. Finally, in Fig. 3 we give the plots of E_l and E_φ versus time corresponding to open and closed PSS trajectories close to the stable 6:1 fixed point for system 1 for $V = 200\,\mathrm{cm}^{-1}$. One observes that the energies undergo two types of oscillations: one is fast and one is slow. The characteristic times for the former type of energy oscillations coincide with the CH-stretching periods and are of the order of 10 fs. The latter type is a kind modulation of the energy exchanges between stretching and hindered rotation: its characteristic time is about 200 fs for the trajectories A and D in Fig. 3 and about 1000 fs for curve B and its analogs, and is infinity for curve C.

The same characteristics can be seen, in an even more detailed way, by looking at the Fourier power spectra of the trajectories A, B, C, and D of Fig. 3. By power spectrum we mean the following function of the frequencies [13]:

$$S(\omega) = |x(\omega)|^2 + |y(\omega)|^2 + |z(\omega)|^2\ ,$$

where

$$x(\omega) = \lim_{T\to\infty} (1/2T) \int_{-T}^{T} l(t) \sin\theta \cos\varphi(t) \exp(-i\omega t) dt$$

$$y(\omega) = \lim_{T\to\infty} (1/2T) \int_{-T}^{T} l(t) \sin\theta \sin\varphi(t) \exp(-i\omega t) dt$$

$$z(\omega) = \lim_{T\to\infty} (1/2T) \int_{-T}^{T} l(t) \cos\theta \exp(-i\omega t) dt$$

We report the results for the four trajectories A, B, C, and D of Fig. 3 in Fig. 4. The integration times were $T = 32768$fs with a 0.05fs step, when solving the Hamilton equations of motion, and the Fourier analysis was conducted by a Fast-Fourier-transform based computer program over the same time, T, using a step size of 1 fs. In Fig. 4 we have reported the results for the three spectral regions with the major Fourier components: between them there is no component above the noise of the calculations, and the stretching overtone regions calculated beyond them are not reported for reasons of conciseness. Looking at the rotational fundamental region (the four plots in the first column),

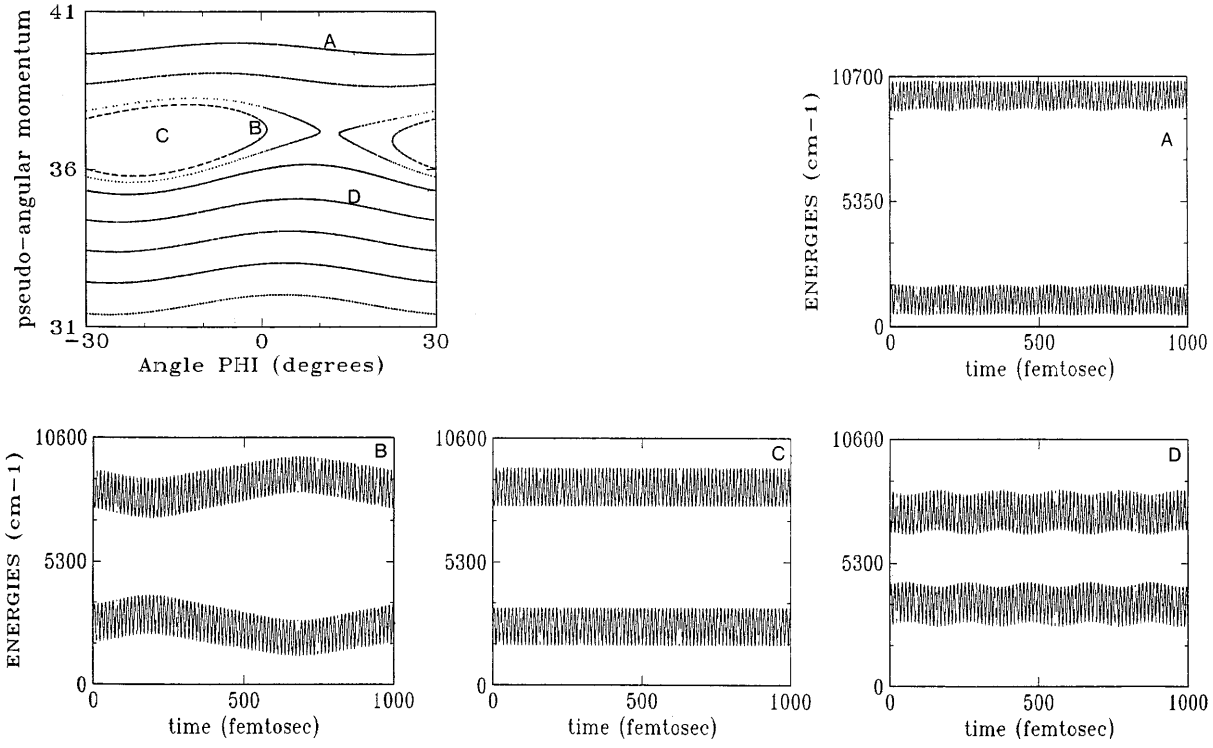

Fig. 3. Portion of the PSS of Fig. 1 *top left* close to the 6:1 resonance ($V = 200\,\mathrm{cm}^{-1}$). Time dependence of rotational and stretching energies E_l and E_φ corresponding to the marked PSS curves. In each plot E_l versus time always corresponds to the *lower trace*; E_φ versus time always corresponds to the *upper trace*

one sees that trajectories A and D show an intense line at $491\,\mathrm{cm}^{-1}$ and $421\,\mathrm{cm}^{-1}$, respectively; for trajectories B and C this line is at $453\,\mathrm{cm}^{-1}$ and is in exact 6:1 resonance with the CH-stretching central line at $2717\,\mathrm{cm}^{-1}$ (second column of Fig. 4). All the aforementioned lines correspond to the rotation frequency ω_R. Close to the line at ω_R, for trajectory B there are two quite evident components at $\omega_\mathrm{R} \pm \omega_\mathrm{M}$, with $\omega_\mathrm{M} = 33\,\mathrm{cm}^{-1}$: the latter corresponds to the long-term modulation observed in the plot of energy versus time in Fig. 3. The shorter-time modulations observed for trajectories A and D produce lines at about $250\,\mathrm{cm}^{-1}$ with intensities too low to be observed in this and the following regions. Going next to the CH-stretching fundamental region, for trajectories A, C, and D three lines are observed, the central one corresponding to the pure CH stretching at ω_S, since the $z(\omega)$ component contributes. The two side components are found at $\omega_\mathrm{S} \pm \omega_\mathrm{R}$ and are generated by $|x(\omega)|^2 + |y(\omega)|^2$; the intensity ratio of the central component to the sum of the side components is $\cos^2\theta / \sin^2\theta$; for the exact resonant trajectory C the two side components have equal intensity. For B-type trajectories the long-term modulation produces further side lines at $\omega_\mathrm{S} + \omega_\mathrm{R} \pm \omega_\mathrm{M}$. Finally, in the first CH-stretching overtone region one observes for all trajectories three lines at $2\omega_\mathrm{S}$ and $2\omega_\mathrm{S} \pm \omega_\mathrm{R}$; for trajectory B satellite lines are observed that differ in frequency from those just mentioned by $\pm n\omega_\mathrm{M}$, where n is an integer. The same phenomena are observed for higher CH-stretching overtone regions, that we do not report here. The consideration of the Fourier power spectrum is useful for further elucidating the dynamical behavior and may help to give an idea of the spectroscopic manifestation of the resonant modes that we have found; however, we feel that it is premature to dwell on this point now.

2.2 Perturbation treatment

We wish to discuss here a perturbative treatment, by which the main findings from the numerical calculations expounded in Sect. 2.1 are rationalized. In the following, we discuss the Hamiltonian of system 1: system 2 can be treated analogously. We first made an approximation to the Hamiltonian function (Eq. 1) by substituting $l = l_0 + (l - l_0)$ into Eq. (3), developing $(l/\mathscr{I})$ in a Taylor series, and keeping the lowest term in $(l - l_0)$.[1] We thus obtained the following partitioning of the Hamiltonian function:

$$H = H_0 + H_1 + H_2 \ , \tag{5}$$

where

$$H_0 = (p^2/2m) + hcD\{1 - \exp[-a(l - l_0)]\}^2 + p_\varphi^2/2\mathscr{I}_0 \tag{6}$$

$$H_1 = -(2/3)(p_\varphi^2/2\mathscr{I}_0)[(l - l_0)/l_0] \tag{7}$$

$$H_2 = hc(V/2)(1 - \cos 6\varphi) \tag{8}$$

[1] Developing $(1/\mathscr{I})$ in a power series of $(\Delta l/l_0)$, one obtains $(p_\varphi^2/2\mathscr{I}_0)[1 - (2\Delta l/3l_0) + (\Delta l/3l_0)^2]$ for the mass values used for CH_3. In the following we stopped at the linear power of $(\Delta l/l_0)$

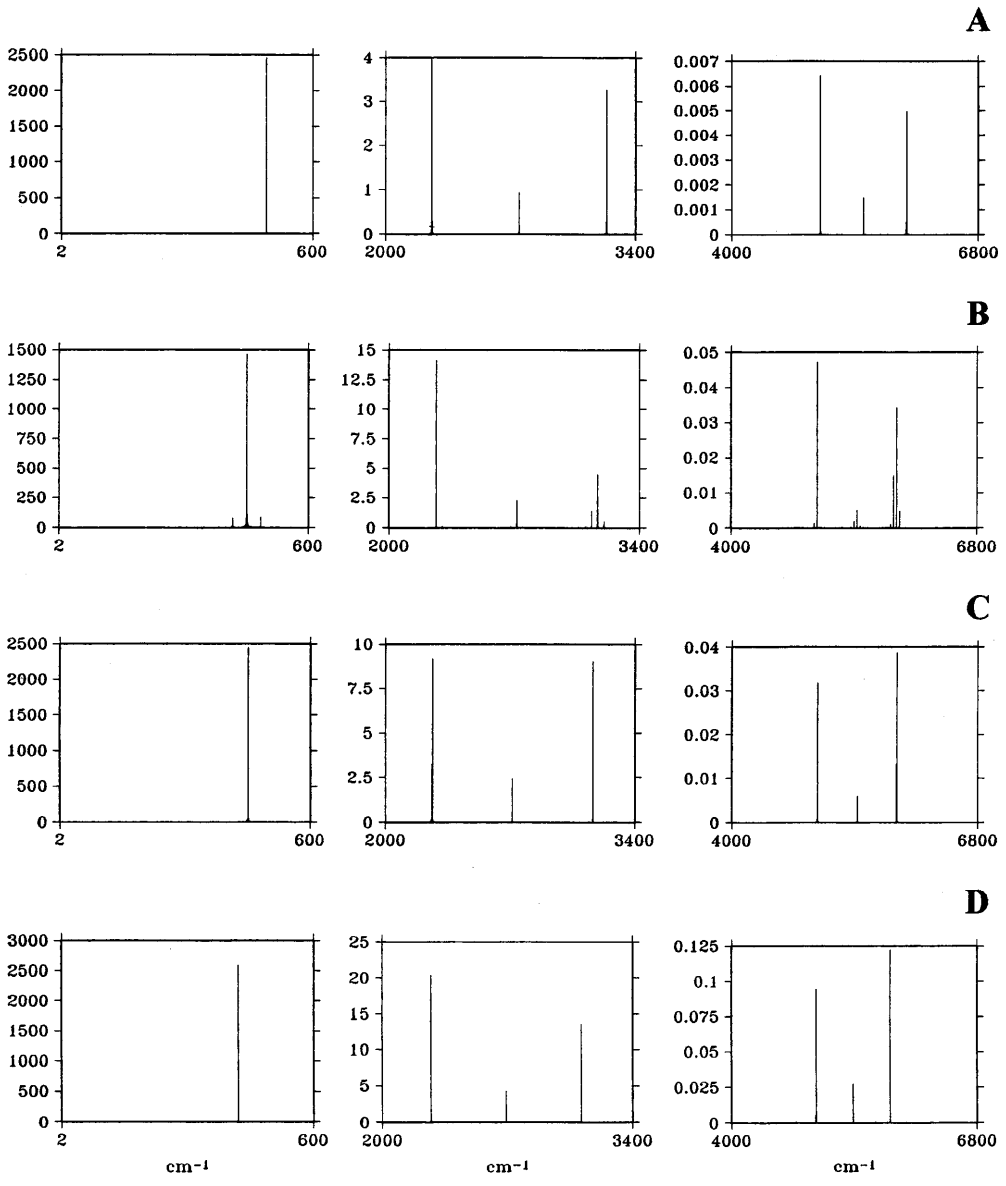

Fig. 4. Fourier power spectra $S(\omega)$ of the trajectories A, B, C, and D presented in Fig. 3. Only the fundamental regions for the pseudorotation and stretching and the first overtone of the stretching are presented. The units for the ordinate axis are arbitrary, of course the relative values between different spectral regions are well defined

H_0 is integrable and can be expressed in terms of the dimensionless actions of the free rotator (p_φ) and the Morse oscillator (J), i.e.

$$H_0 = (\mathscr{B}/3)p_\varphi^2 + (\omega_0 - \chi J)J \ , \tag{9}$$

where $\mathscr{B}$ is the CH-bond rotational constant in wavenumber units for rotations around CX, i.e. $\mathscr{B} = (3h/8\pi^2 c\mathscr{I}_0)$, and for the parameters adopted here its value is 18.97 cm^{-1}. The angle coordinates conjugated to p_φ and J are φ and Φ (the latter denotes the phase of the stretching coordinates l) and do not appear in H_0. The frequencies of the separated rotational and stretching motions can be calculated from the relations [12]

$$\omega_R(p_\varphi) = (\partial H_0/\partial p_\varphi) = (2\mathscr{B}/3)p_\varphi \tag{10}$$

$$\omega_S(J) = (\partial H_0/\partial J) = \omega_0 - 2\chi J \tag{11}$$

It is convenient to write H_1 in terms of action/angle variables; we verified that it is not necessary to use the Morse actions and angles [20, 21], but just the corresponding harmonic quantities [12]. In this way (working with dimensionless action, J, and wavenumber units for ω_0)

$$(l - l_0) = \sqrt{(hJ/2\pi^2 mc\omega_0)}\sin\Phi = \kappa\sqrt{J}\sin\Phi \tag{12}$$

(for the present case $\kappa = 0.15$ Å).

By substituting into Eq. (7), we obtain

$$H_1 = -\mathscr{A}p_\varphi^2\sqrt{J}\sin\Phi \ ,$$

where $\mathscr{A} = (2/9)\mathscr{B}(\kappa/l_0) = 0.632\,\text{cm}^{-1}$.

The three terms in Eq. (5), that have been rewritten in terms of action/angle variables, have different importance in different regimes. H_2 is responsible for librations of the angle φ; the magnitude of V gives the portion of phase space occupied by librational modes (the six curves at low p_φ in Fig. 1). The regime of these modes is accounted for by just $(H_0 + H_2)$, which is separable. We

are going to present a perturbative treatment for the nonseparable Hamiltonian $(H_0 + H_1 + H_2)$, with the aim of justifying locally the rotational regime, in the region which comprises the 6:1 resonance. The perturbative treatment allows $(H_0 + H_1 + H_2)$ to be transformed to a Hamiltonian, Z, depending on just one angle; the validity of such a perturbative approach cannot be extended globally to the whole phase space. The perturbation scheme we apply is based on the Lie series [12, 14]: we rewrite the Hamiltonian function (Eq. 5) as follows:

$$H(\varphi, \Phi, p_\varphi, J) = h_0(p_\varphi, J) + \varepsilon f(\varphi, \Phi, p_\varphi, J) \ , \tag{13}$$

where

$$h_0(p_\varphi, J) = \omega_0 J + (p_\varphi^2/2\mathscr{I}_0) \tag{14}$$

is the unperturbed Hamiltonian and

$$\begin{aligned} \varepsilon f(\varphi, \Phi, p_\varphi, J) = &-\chi J^2 + (V/2)(1 - \cos 6\varphi) \\ &- \mathscr{A}\sqrt{J} p_\varphi^2 \sin \Phi \end{aligned} \tag{15}$$

is the perturbation term. In the hypothesis of high p_φ all three perturbative terms are equally important. Following Ref. [14], we look for a canonical transformation: $(p, q) \to (p', q')$ of the form

$$\begin{aligned} (p, q) = \exp(\varepsilon L_w)(p', q') &= (p', q') + \varepsilon\{w, (p', q')\} \\ &+ (\varepsilon^2/2)\{w, \{w, (p', q')\}\} \ , \end{aligned} \tag{16}$$

where the symbol $\{\ldots, \ldots\}$ stands for Poisson brackets [12, 14]. The Hamiltonian function H of Eq. (13) transforms to

$$\begin{aligned} H' &= \exp(\varepsilon L_w) H \\ &= H + \varepsilon\{w, H\} + (\varepsilon^2/2)\{w, \{w, H\}\} \end{aligned} \tag{17}$$

with truncation at the second order in ε.

Substituting Eq. (13) for H, one obtains

$$H' = h_0 + \varepsilon f + \varepsilon\{w, h_0\} + \varepsilon^2(\{w, f\} + \tfrac{1}{2}\{w, \{w, h_0\}\}) \ . \tag{18}$$

At this point one has to determine the generating function w in such a way that the lowest-order term in ε depends on actions only. This is possible because no resonance appears at this order. One has

$$f + \{w, h_0\} = Z(p_\varphi, J) \ . \tag{19}$$

w is then expanded in a Fourier series, i.e.

$$w = \sum_{jk} c_{jk}(p_\varphi, J) \exp[i(j\Phi + k\varphi)] \ , \tag{20}$$

where j and k run over the entire set of relative integer numbers. Substituting Eq. (20) into Eq. (19), one obtains

$$\begin{aligned} w = &-i(V\mathscr{I}_0/24p_\varphi)(\mathrm{e}^{i6\varphi} - \mathrm{e}^{-i6\varphi}) \\ &- (\mathscr{A}\sqrt{J}/2\omega_0) p_\varphi^2 (\mathrm{e}^{i\Phi} + \mathrm{e}^{-i\Phi}) \ . \end{aligned} \tag{21}$$

Applying Eq. (21) in the Poisson brackets required by the next order in ε of Eq. (18), one obtains the following equations for H':

$$H' = h'(p_\varphi, J) + \varepsilon^2 f'(\varphi, \Phi, p_\varphi, J) \ , \tag{22}$$

where

$$\begin{aligned} h'(p_\varphi, J) = h_0(p_\varphi, J) + \varepsilon Z(p_\varphi, J) &= \omega_0 J \\ &+ (p_\varphi^2/2\mathscr{I}_0) - \chi J^2 + (V/2) \end{aligned} \tag{23}$$

and

$$\begin{aligned} \varepsilon^2 f'(\varphi, \Phi, p_\varphi, J) = &-(\mathscr{A}^2 p_\varphi^4/4\omega_0) + (V^2\mathscr{I}_0/16p_\varphi^2) \\ &- (V^2\mathscr{I}_0/32p_\varphi^2)(\mathrm{e}^{i12\varphi} + \mathrm{e}^{-i12\varphi}) \\ &- (i\chi\mathscr{A}(J)^{3/2} p_\varphi^2/\omega_0)(\mathrm{e}^{i\Phi} - \mathrm{e}^{-i\Phi}) \\ &- (iV\mathscr{A}\sqrt{J}/2)[-(\mathscr{I}_0/4) + (3p_\varphi/2\omega_0)] \\ &\times (\mathrm{e}^{i(6\varphi+\Phi)} - \mathrm{e}^{-i(6\varphi+\Phi)}) \\ &- (iV\mathscr{A}\sqrt{J}/2)[(\mathscr{I}_0/4) + (3p_\varphi/2\omega_0)] \\ &\times (\mathrm{e}^{i(6\varphi-\Phi)} - \mathrm{e}^{-i(6\varphi-\Phi)}) \ . \end{aligned} \tag{24}$$

Next, we seek another canonical transformation w' to coordinates and momenta (p'', q'') such that the transformed Hamiltonian H'' is of the form

$$H'' = h' + \varepsilon^2(f' + \{w', h'\}) \ . \tag{25}$$

As done previously for w, we require that the new generating function w' be expandable in a Fourier series

$$w' = \sum_{jk} c'_{jk}(p_\varphi, J) \exp[i(j\varphi + k\Phi)] \tag{26}$$

(j, k run over all relative integer numbers). Again, we require that

$$f' + \{w', h'\} = Z' \ . \tag{27}$$

Notice that Z' can be imposed to be dependent on actions only, if no resonance appears. Indeed the series

$$\begin{aligned} \{w', h'\} &= -i \sum_{jk} c'_{jk} \exp[i(j\varphi + k\Phi)] \\ &\quad \times [j(p_\varphi/\mathscr{I}_0) + k(\omega_0 - 2\chi J)] \\ &= -i \sum_{jk} c'_{jk} \exp[i(j\varphi + k\Phi)] \\ &\quad \times [j\omega_{\mathrm{R}}(p\varphi) + k\omega_{\mathrm{S}}(J)] \end{aligned} \tag{28}$$

shows zero factors in correspondence $6\omega_{\mathrm{R}} = \omega_{\mathrm{S}}$, namely for $j = 6$ and $k = -1$. For this reason one must set the coefficients c'_{-61} and c'_{61} equal to zero. From Eq. (27) we determine Z' from f' [14]: since we are only interested in investigating the properties of the transformed Hamiltonian close to the resonance, we do not report explicitly the coefficients c'_{jk} that we have calculated in view of studying the other resonances of Figs. 1 and 2. In conclusion we obtain

$$\begin{aligned} H'' = &\omega_0 J + (p_\varphi^2/2\mathscr{I}_0) - \chi J^2 + (V/2) - (\mathscr{A}^2 p_\varphi^4/4\omega_0) \\ &+ (V^2\mathscr{I}_0/16p_\varphi^2) \\ &+ (V\mathscr{A}\sqrt{J})[(\mathscr{I}_0/4) + (3p_\varphi/2\omega_0)] \sin(6\varphi - \Phi) \end{aligned} \tag{29}$$

Finally we make the following canonical transformation

$$\theta_R = 6\varphi - \Phi \quad I_R = p_\varphi/6 \quad \theta = \Phi \quad I = J + (p_\varphi/6) \tag{30}$$

that is commonplace in the instance of resonances [12]. From Eq. (29) we obtain

$$\begin{aligned} H''(I, I_R, \theta_R) = {} & \omega_0(I - I_R) - \chi(I - I_R)^2 + (V/2) \\ & + 18I_R^2/\mathscr{I}_0 - (\mathscr{A}^2 6^4 I_R^4/4\omega_0) \\ & + (V^2\mathscr{I}_0/576I_R^2) \\ & + (V\mathscr{A}\sqrt{(I - I_R)}) \\ & \times [(\mathscr{I}_0/4) + (9I_R/\omega_0)] \sin\theta_R \ . \end{aligned} \tag{31}$$

A systematic analytical study of Eq. (31) is hard and is not terribly rewarding; however, a few qualitative and firm conclusions are possible:

1. Equation (31) is the sum of an angle-independent part and of an oscillating part: the relative weight of the latter with respect to the former determines whether or not there is the resonance we encountered in the numerical analysis.

2. The fixed points of H'' (when the resonance is present) are for $\theta_R = \pm(\pi/2)$, which is quite close to what we have found numerically. Indeed, from Eq. (30), setting $\Phi = 0$, one obtains $\varphi = \pm(\pi/12)$, which is very close to the result of Fig. 1; instead, setting $\varphi = 0$, one obtains $\Phi = \pm(\pi/2)$, namely $l - l_0$ of Eq. (12) at the minimum and maximum value, respectively. To be more precise though, one should remember that the conjugated coordinates and momenta to be used in Eq. (30) are not the original ones: consequently, in order to make a comparison with the numerical experiments, one must transform twice the canonical coordinates through Eq. (16) with the Lie series transformation generated by w (Eq. 21) and w' (Eq. 26). Up to the first order in ε, the transformation for the φ coordinate reads

$$\begin{aligned} \varphi = {} & \varphi'' + (V\mathscr{I}_0/12p_{\varphi''}^2)\sin 6\varphi'' \\ & + 2(\mathscr{A}\sqrt{J''}/\omega_0)p_{\varphi''}\cos\Phi'' \ , \end{aligned} \tag{32}$$

where we denote the transformed coordinates and momenta by use of the second primes. Substituting in Eq. (32) the values for φ'' and $p_{\varphi''}$ of the fixed points, that have been obtained graphically, as described later one obtains $\varphi = -15.5°$ and $\varphi = +14.5°$, which is even closer to the numerical experiment.

In order to study the stability of the fixed points and to investigate whether Eq. (31) is quantitatively in good correspondence with the numerical experiments, we have plotted the level curves $H''(I, I_R, \theta_R) = E$ at fixed values for I, in the ranges $I_R \in (1, I)$ and $\theta_R \in (-\pi, +\pi)$. I has the meaning of the sum of the vibrational and pseudo-rotational actions (the latter one divided by 6). In order to seek a correspondence with the calculations of Fig. 1, we have determined J and p_φ at the lowest order of approximation from a slightly modified version of Eq. (14) by setting $h_0 = E$, namely

$$E = \omega_0 J - \chi J^2 + (p_\varphi^2/2\mathscr{I}_0) \ . \tag{33}$$

Corresponding to the values $E = 2940$, 4365, 5760, 7125, 8460, 9765, 11040, and 12285 cm^{-1}, we obtain the maximum value for J, i.e. $J = 1$, 1.5, 2, 2.5, 3, 3.5, 4, and 4.5 (for $p_\varphi = 0$) and the maximum value for p_φ, i.e. p_φ = 21.56, 26.27, 30,18, 33.56, 36.57, 39.29, 41.78, and 44.07 (for $J = 0$), respectively, in dimensionless units. Such values correspond to the transition orders $\Delta v = 1, 2, 3, 4, 5, 6, 7, 8$. In Fig. 5 we report the plots for $I = 5.59$ ($\Delta v = 4$) (top) and $I = 6.96$ ($\Delta v = 7$) (bottom) which can be obtained by substituting $J = 0$ and $p_\varphi = 33.56$ and 41.78, respectively, in Eq. (30). Indeed such an approximation is permissible since the 6:1 resonances are found for high values of the pseudorotational action p_φ. We see that in the first case only open curves are present, whereas in the second case closed curves also appear centered at $\theta_R = -(\pi/2)$. For open curves θ_R, given by Eq. (30), can vary from $-\pi$ to π.

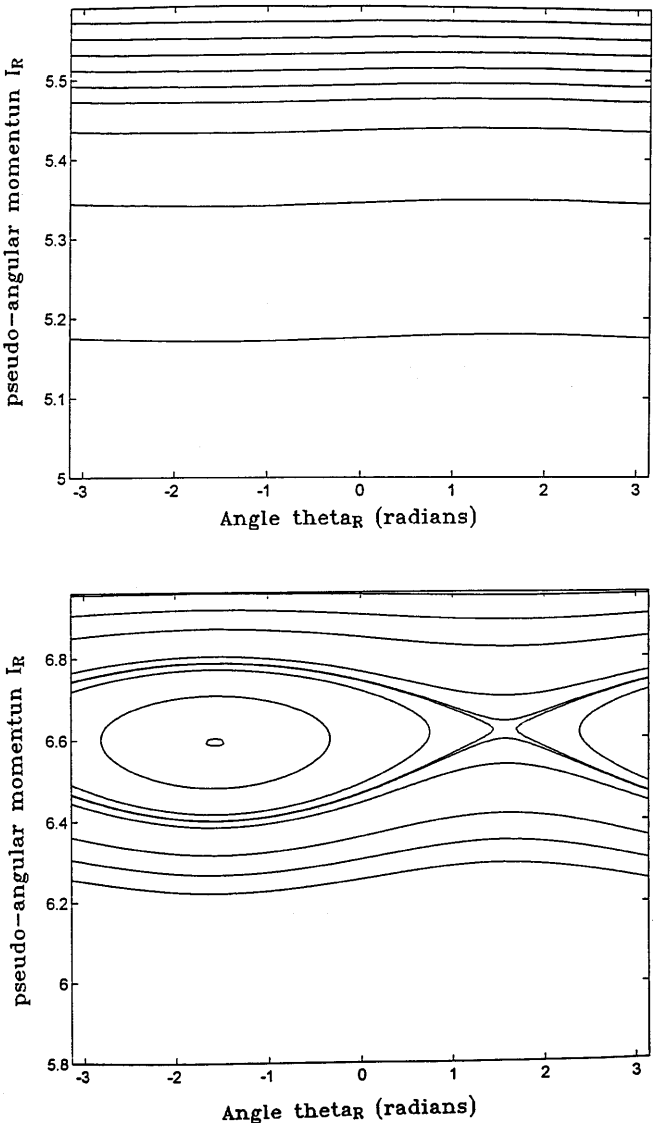

Fig. 5. Contour plots for the transformed Hamiltonian $H''(I, I_R, \theta_R)$ obtained by the perturbative treatment presented in the text. The plots are in the (I_R, θ_R) plane at a fixed value for I. A limited portion is shown in the ordinate axis. Two plots are shown corresponding to the two values $I = 5.59$ (*top*) and $I = 6.96$ (*bottom*). I_R and I are in dimensionless units

Namely, there is no relation between the phase of the stretching vibration Φ and the phase of the pseudorotation φ: consequently these curves correspond to the usual "free" rotations. On the other hand, for closed curves θ_R varies in a limited interval, giving rise to a phase locking of stretching and rotation; even though φ varies between $-\pi$ and π, meaning that we are still in the presence of a full rotation. In the largest closed curve there is a strong oscillation in I_R, i.e. in p_φ according to Eq. (30) meaning that the rotational energy, E_φ, undergoes a periodic variation, with a long period, as observed in Fig. 3B (and as confirmed by the Fourier cross spectrum in Fig. 4B). The perturbative treatment is consistent with the numerical results also in that the stable fixed point is predicted at $\theta_R = -(\pi/2)$, while the unstable one is predicted at $\theta_R = +(\pi/2)$. Furthermore the values for resonant action, I_R, are close to the maximum allowed value, i.e. to I. Indeed by the perturbative treatment we found that I_R at both fixed points is 6.6 in dimensionless units for $\Delta v = 7$ (Fig. 5, bottom). This value compares well with the value for $p_\varphi/6$ found numerically, namely 6.15; however, by the perturbative treatment two slightly different values for I_R are found at the stable and unstable fixed points, whereas just one is found by the numerical experiment. Also, the transition from the regime described in the top part of Fig. 5 to the regime described in the bottom part of Fig. 5 is found at $\Delta v = 6$. This is not too far from what has been found numerically.

In conclusion we feel that a qualitatively general agreement and a quantitative agreement of the order of 90% has been achieved by the perturbative treatment used here. We have pointed out several instances where approximations have been made and better quantitative agreement may be reached, for example, by using Morse actions and angles instead of harmonic ones and also by making a more accurate expansion of $1/\mathscr{I}$.[1,2] More importantly, we feel that the above perturbative treatment can help considerably to understand the case of methanol, with due changes in resonance terms (see Fig. 2). This is trivially true for the resonance $\omega_S = 3\omega_R$ at high Δv, but also for the resonances at various orders showing up at much lower Δv and persisting (see Fig. 2 again) at higher Δv.

3 Conclusions

We have investigated the vibrational classical dynamics of a librating/rotating methyl group with just two degrees of freedom: the hindered rotation φ and the stretching $l - l_0$ in the methyl group (and in the oxydril group in the case of methanol) for typical energies of spectroscopic interest. We neglected any influence from overall molecular rotations. The assumed coupling between the two vibrational coordinates is just in the kinetic energy and is usually given little attention. We have found that this coupling can give rise to interesting features in the dynamics: besides the torsional and rotational modes, there is a third type of mode, namely resonant rotational modes. The two former ones are adiabatic, namely the angle φ coordinate is qualitatively decoupled from the other vibrational motions. Instead, the resonant rotational states are evidently nonadiabatic. These modes arise from the synchronization that takes place between stretching vibrations and rotations, originating from the strong centrifugal force generated by the rapid rotation of the methyl or the oxydril group. We think that these modes may have some influence on the CH-overtone spectra, since their Fourier spectrum is markedly different from that of "neighboring" rotational states. The perturbation treatment provided in this work will help in this specific respect, since it can provide the invariant actions of the perturbed motions, which are relevant for the semiclassical quantization of the new actions [22]. Moreover it well describes the phase locking between stretching and hindered rotation.

It appears at the moment that these "new" modes are predicted for high values of the hindered rotational action and, consequently, for high quantum numbers: indeed we have evaluated that for a toluene-type molecule it is of the order of 36, while for methanol it is either of the order of 25 or 20. Furthermore, we have observed higher-order resonances for energies corresponding to lower hindered rotation quantum number. The latter modes are in an accessible spectroscopic range and we have started to study them by the same approach expounded here. In particular the perturbative treatment will be applied to higher orders in order to study all possible resonances in methanol and to a modified Hamiltonian contemplating also an interaction term in the potential energy between the two degrees of freedom, as strongly suggested in the literature [1–3, 6, 7].

Acknowledgements. We gratefully acknowledge help from Antonio Giorgilli at Dipartimento di Matematica, Università di Milano, for helping us to apply correctly the Lie series perturbative approach.

[2] Substituting for the harmonic action-angle dependence in the first omitted term discussed in Footnote 1, one obtains $(p_\varphi^2/2\mathscr{I}_0)(\kappa^2/9I_0^2)J\sin^2\Phi = \mathscr{A}'' p_\varphi^2 J \sin^2\Phi$. With the values used in the calculations the constant $\mathscr{A}''$ is $0.015\,\mathrm{cm}^{-1}$

References

1. Cavagnat D, Lascombe J (1982) J Mol Spectrosc 92: 141
2. Cavagnat D, Lespade L, Lapouge C (1995) Ber Bunsenges Phys Chem 99: 544
3. Cavagnat D, Lespade L (1997) J Chem Phys 106: 7946
4. Martens CG, Reinhardt WP (1990) J Chem Phys 93: 5621
5. (a) Moss DB, Parmenter CS (1993) J Chem Phys 98: 6897; (b) Timbers PJ, Parmenter CS, Moss DB (1994) J Chem Phys 100: 1028
6. Li-Hong Xu (1998) How much do we know (and still need to learn) about the methanol molecule. Talk RA01 at the 53rd International Conference on Molecular Spectroscopy, Columbus, OH, USA, 1998
7. (a) Rizzo TR, Boyarkin OV, Schmid M, Chirokolava A, Perry DS (1998) Spectroscopy and dynamics of highly vibrationally excited methanol. Note FA1 presented at the 53rd International Conference on Molecular Spectroscopy, Columbus, Ohio, 1998; (b) Perry DS, Boyarkin OV, Rizzo TR (1998) Torsional analysis of methanol in the vibrational manifold up to $v_{OH} = 6$. Note RA 10 presented at the 53rd International Conference on Molecular Spectroscopy, Columbus, Ohio, 1998

8. Dittrich W, Reuter M (1994) Classical and quantum dynamics. From classical paths to path integrals, 2nd edn. Springer, Berlin Heidelberg New York
9. (a) Schranz HW, Collins MA (1993) J Chem Phys 98: 1132; (b) Schranz HW, Collins MA (1994) J Chem Phys 101: 307
10. Watson JKG (1977) In: Durig JR (ed) Vibrational spectra and structure. Elsevier, Amsterdam, pp 1–89
11. McKean DC, Watt RA (1976) J Mol Spectrosc 61: 184
12. Lichtenberg AJ, Lieberman MA (1992) Regular and chaotic dynamics, 2nd edn. Applied Mathematics Sciences series, vol 38. Springer Berlin Heidelberg New York
13. Noid DW, Koszykowski ML, Marcus RA (1977) J Chem Phys 67: 404
14. Giorgilli A (1995) In: Roy AE, Steves BD (eds) From Newton to chaos: modern techniques for understanding and coping with chaos in *N*-body dynamical systems. Plenum New York, pp 21–28
15. Wilson EB, Jr Decius J, Cross PC (1955) Molecular vibrations. McGraw-Hill, New York
16. Zhu C, Kjaergaard HG, Henry BR (1997) J Chem Phys 107: 691
17. Cavagnat D, Lautie MF (1990) J Raman Spectrosc 21: 185
18. Henry BR (1981) In: Durig JR (ed) Vibrational spectra and structure, vol 10. Elsevier, New York, p 269
19. (a) Heisenberg W (1949) The physical principles of quantum theory. Dover New York; (b) Koszykowski ML, Noid DW, Marcus RA (1982) J Chem Phys 86: 2113
20. Jaffé C, Brumer P (1980) J Chem Phys 73: 5446
21. Longhi G, Abbate S, Zagano C, Botto G, Ricard-Lespade L (1992) Theor Chim Acta 82: 321
22. Percival IC (1977) Adv Chem Phys 36: 1